

Spatial quantum coherent modulation with perfect hybrid vector vortex beam based on atomic medium

Yan Ma(马燕), Xin Yang(杨欣), Hong Chang(常虹), Xin-Qi Yang(杨鑫琪), Ming-Tao Cao(曹明涛), Xiao-Fei Zhang(张晓斐), Hong Gao(高宏), Rui-Fang Dong(董瑞芳), and Shou-Gang Zhang(张首刚)
Citation: Chin. Phys. B, 2024, 33 (**2**): 024204. DOI: 10.1088/1674-1056/ad0f86
Journal homepage: http://cpb.iphy.ac.cn; http://iopscience.iop.org/cpb

What follows is a list of articles you may be interested in

Terahertz quasi-perfect vortex beam with integer-order and fractional-order generated by spiral spherical harmonic axicon

Si-Yu Tu(涂思语), De-Feng Liu(刘德峰), Jin-Song Liu(刘劲松), Zhen-Gang Yang(杨振刚), and Ke-Jia Wang(王可嘉)
Chin. Phys. B, 2024, 33 (**1**): 014211. DOI: 10.1088/1674-1056/acf91c

Young's double slit interference with vortex source

Qilin Duan(段琦琳), Pengfei Zhao(赵鹏飞), Yuhang Yin(殷玉杭), and Huanyang Chen(陈焕阳)
Chin. Phys. B, 2024, 33 (**1**): 014202. DOI: 10.1088/1674-1056/acfdfd

Ultraviolet metalens and metalens array of focused vortex beams

Jinping Zhang(张金平), Yan Wang(王焱), Huan Yuan(袁欢), Zehao Wang(王泽豪), Yang Deng(邓阳),Chengzhi Huang(黄承志), Jiagui Wu(吴加贵), and Junbo Yang(杨俊波)
Chin. Phys. B, 2023, 32 (**6**): 064206. DOI: 10.1088/1674-1056/ac9d87

Propagation and focusing characteristics of the Bessel-Gaussian beam with the spiral phase term of new power-exponent-phase

Aotian Wang(王傲天), Lianghong Yu(於亮红), Jinfeng Li(李进峰), and Xiaoyan Liang(梁晓燕)
Chin. Phys. B, 2023, 32 (**4**): 044201. DOI: 10.1088/1674-1056/acb1fe

Generation of elliptical airy vortex beams based on all-dielectric metasurface

Xiao-Ju Xue(薛晓菊), Bi-Jun Xu(徐弼军), Bai-Rui Wu(吴白瑞), Xiao-Gang Wang(汪小刚), Xin-Ning Yu(俞昕宁), Lu Lin(林露), and Hong-Qiang Li(李宏强)
Chin. Phys. B, 2023, 32 (**2**): 024215. DOI: 10.1088/1674-1056/ac7cd0

Spatial quantum coherent modulation with perfect hybrid vector vortex beam based on atomic medium

Yan Ma(马燕)[1,2], Xin Yang(杨欣)[3], Hong Chang(常虹)[1,2], Xin-Qi Yang(杨鑫琪)[1,2], Ming-Tao Cao(曹明涛)[1,2,†], Xiao-Fei Zhang(张晓斐)[4], Hong Gao(高宏)[3], Rui-Fang Dong(董瑞芳)[1,2,5,‡], and Shou-Gang Zhang(张首刚)[1,2,§]

[1] *Key Laboratory of Time Reference and Applications, National Time Service Center, Chinese Academy of Sciences, Xi'an* 710600, *China*
[2] *School of Astronomy and Space Science, University of Chinese Academy of Sciences, Beijing* 100049, *China*
[3] *Ministry of Education Key Laboratory for Nonequilibrium Synthesis and Modulation of Condensed Matter, Shaanxi Key Laboratory of Quantum Information and Quantum Optoelectronic Devices, School of Science, Xi'an Jiaotong University, Xi'an* 710049, *China*
[4] *Department of Physics, Shaanxi University of Science and Technology, Xi'an* 710021, *China*
[5] *Hefei National Laboratory, Hefei* 230088, *China*

(Received 23 October 2023; revised manuscript received 21 November 2023; accepted manuscript online 24 November 2023)

The perfect hybrid vector vortex beam (PHVVB) with helical phase wavefront structure has aroused significant concern in recent years, as its beam waist does not expand with the topological charge (TC). In this work, we investigate the spatial quantum coherent modulation effect with PHVVB based on the atomic medium, and we observe the absorption characteristic of the PHVVB with different TCs under variant magnetic fields. We find that the transmission spectrum linewidth of PHVVB can be effectively maintained regardless of the TC. Still, the width of transmission peaks increases slightly as the beam size expands in hot atomic vapor. This distinctive quantum coherence phenomenon, demonstrated by the interaction of an atomic medium with a hybrid vector-structured beam, might be anticipated to open up new opportunities for quantum coherence modulation and accurate magnetic field measurement.

Keywords: perfect hybrid vector vortex beam, topological charge, quantum coherence, optical manipulation

PACS: 42.50.–p, 42.50.Gy, 32.80.Qk, 32.30.Dx **DOI:** 10.1088/1674-1056/ad0f86

1. Introduction

The perfect hybrid vector vortex beam (PHVVB), which has a hybrid information coding capacity and constant ring radius with different topological charges,[1–4] is selected as a popular candidate in various high-dimensional quantum communication protocols.[5–8] Since vector vortex beams (VVBs) are generally generated with vortex half-wave plates and polarization elements,[9,10] their manipulation has mainly been demonstrated with linear optics.[11,12] Recently, VVBs have also been studied for interactions with atomic medium,[13,14] which presents a charming possibility of flexible modulation freedom of VVBs. For instance, VVBs have been studied with high-dimensional information coding in quantum memory,[15] and a novel type of spatial mode selector has also been demonstrated in atom vapor.[16–18]

The magic behind this kind of atom–light interaction modulation is the spatial atomic quantum coherence.[19,20] Principally, quantum coherence occurs in the interaction between light and atoms, which can be realized by two laser beams coupling with a three-level system.[21] When employing the VVBs as the probe beam to interact with the atomic medium, it can imprint the additional vortex phase and angular momentum to the atoms, which makes atom spin spatially different in cross-section regions.

The coherence transporting effect should be considered since the atoms move randomly in the vapor. Xiao *et al.*[22] found that the coherent population can be transferred from site to site among the atoms. Recently, the rapid transport of atomic coherence has also been observed with hybrid VVBs,[23] which can be controlled by an external magnetic field.[24] However, there is no report about the coherent transport with high-order vortex beam, which is essentially crucial for high-dimension coding in atomic ensembles.

In this paper, we experimentally investigate the spatial quantum coherence modulation with a PHVVB in rubidium vapor. We first generate the PHVVB by sending the Gaussian beam through a combination set of an axicon, a double-glued lens, a vortex half-wave plate, and a quarterwave plate. Then, we study the absorption of the PHVVB with different TCs under variant magnetic fields. We find that the transmission spectrum linewidth of PHVVB can be effectively maintained regardless of the TC. Still, the width of transmission peaks increases slightly as the beam size expands in hot atomic vapor. We believe our results can be helpful for demonstrating the high-dimension coding with PHVVB in atomic ensembles.

2. Experimental setup and measurement of Stokes parameters

The schematic diagram of the experimental setup is shown in Fig. 1(a). The laser beam from an external cavity

†Corresponding author. E-mail: mingtaocao@ntsc.ac.cn
‡Corresponding author. E-mail: dongruifang@ntsc.ac.cn
§Corresponding author. E-mail: szhang@ntsc.ac.cn

© 2024 Chinese Physical Society and IOP Publishing Ltd

diode laser (Toptica DL pro) with a wavelength of 780 nm is divided into two parts by a polarization beam splitter (PBS). One part locks the laser frequency using the saturated absorption spectrum (SAS), while the other is coupled into a single-mode fiber to generate a standard Gaussian beam. We use an axicon after the single-mode fiber to produce the Bessel beam. The perfect vortex beam is obtained by Fourier transforming the Bessel beam through a double-glued lens,[25,26] as shown in Fig. 1(c). After that, we send the perfect vortex beam through a Q-plate to generate PVVB.

Furthermore, using an additional quarter-wave plate (QWP), we can convert PVVB to the PHVVB, which travels through a vapor cell with isotopically enriched ^{85}Rb. The vapor cell is located in a three-layer μ-metal magnetic shield, with a solenoid coil inside the inner layer, which provides a uniform bias magnetic field to induce the Zeeman splitting. The temperature is set to approximately 65 °C to increase the atomic density. After passing through the vapor cell, the profile of PHVVB is recorded by a charge-coupled device camera (CCD).

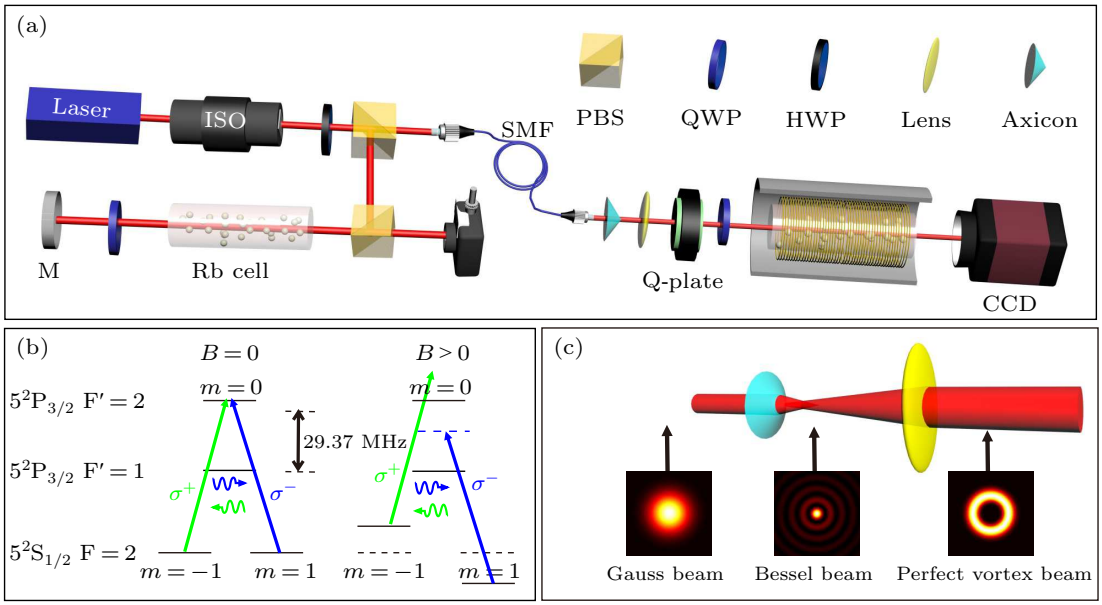


Fig. 1. (a) The experimental setup. PBS: polarization beam splitter; QWP: quarter-wave plate; HWP: half-wave plate; SMF: single-mode fiber; CCD: charge-coupled device camera. (b) Schematic diagram of energy levels with/without magnetic field. σ^+: right-hand polarization beam; σ^-: left-hand polarization beam. (c) Setup for perfect vector vortex beam generation.

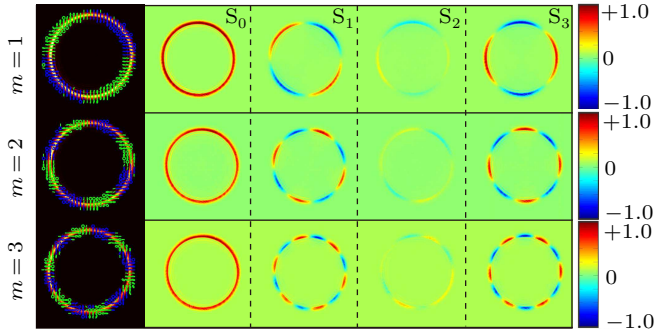


Fig. 2. The polarization distribution (first column, blue: left-hand circular polarization; green: right-hand circular polarization) and the normalized Stokes parameters of PHVVB, corresponding to the Q-plate with $m = 1$, 2, 3, respectively.

Firstly, we analyze the polarization state of the generated PHVVB. To effectively quantify the transverse spatial polarization distribution of PHVVB carrying various TCs, in the case of Q-plate with $m = 1, 2, 3$, respectively, we experimentally measure the horizontal, vertical, diagonal, anti-diagonal, left and right circular polarization components of the PHVVB by utilizing a combination of wave plates and PBS.[27] The values of each Stokes parameter ($S = [S_0, S_1, S_2, S_3]$) can be calculated with the following equations:

$$\begin{aligned} S_0 &= I_{\mathrm{H}} + I_{\mathrm{V}} = I(0^\circ, 0^\circ) + I(90^\circ, 0^\circ), \\ S_1 &= I_{\mathrm{H}} - I_{\mathrm{V}} = I(0^\circ, 0^\circ) - I(90^\circ, 0^\circ), \\ S_2 &= I_{\mathrm{A}} - I_{\mathrm{D}} = I\left(45^\circ, 0^\circ\right) - I\left(135^\circ, 0^\circ\right), \\ S_3 &= I_{\mathrm{R}} - I_{\mathrm{L}} = I\left(135^\circ, 90^\circ\right) - I\left(45^\circ, 90^\circ\right), \end{aligned} \tag{1}$$

where $I(\alpha, \beta)$ denotes the intensity when the HWP and QWP rotated by the angle relative to their fast axis.

Therefore, the normalized Stokes parameters $S_i = S_i/S_0$ ($i = 1, 2, 3$) can be obtained, as depicted in Fig. 2. And the polarization distribution of the PHVVB can also be reconstructed,[28] as presented in the first column.

3. Experimental results and analysis

Following that, we turn to the interaction between the PHVVB and the Rb atoms. In our scheme, the laser frequency is locked to the transition of $5S_{1/2}, F = 2 \rightarrow 5P_{3/2}, F' = 2$ of ^{85}Rb D_2 line.[29] The schematic energy transition diagram is depicted in Fig. 1(b). When an axial magnetic field is applied, the Zeeman effect induces the splitting of the hyperfine energy

levels in the atomic system. Each Zeeman sublevel $|F,m_F\rangle$ shifts by an amount $\mu_B g_F m_F B$, where $\mu_B = 1.4$ MHz/Gauss is the Bohr magneton, g_F is the Landé g-factor, and B is the magnetic field strength. In the experiment, the beam with σ^+ polarization couples the Zeeman sublevel transition $|m=-1\rangle \rightarrow |m=0\rangle$, and σ^- polarization couples the $|m=1\rangle \rightarrow |m=0\rangle$ transition.

In the experiment, we define the quantization axis as the propagation direction along the beam. As shown in Fig. 3(a), when increasing the positive magnetic field, the transmitted intensity gets brighter along the 45° diagonal direction while gets dimmer along the −45° anti-diagonal direction. Figures 3(b) and 3(c) are the results with $m=2$ and $m=3$, respectively.

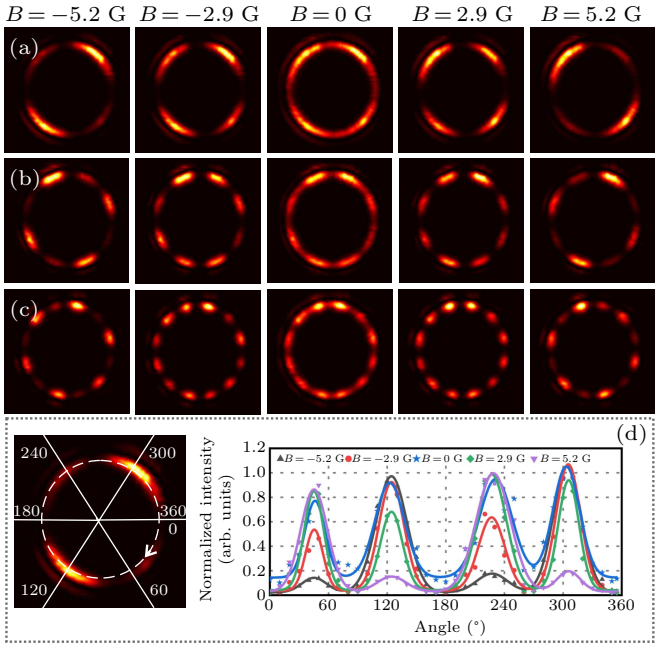


Fig. 3. The intensity profiles of the PHVVB transmitted through the Rb atomic medium at different magnetic field strengths. Panels (a)–(c) corresponding to the results for beams with different topological charges $m=1$, $m=2$, and $m=3$. (d) Normalized intensity dependence of azimuth angle with $m=1$.

As the magnetic field increases in the positive direction, the Zeeman splitting of the ground state is three times than that of the excited state. Consequently, the σ^+ beam experiences a shift from resonance to blue detuning, which results in weakened absorption and enhanced transmission of the σ^+ polarized beam. Moreover, the σ^- polarized beam gets closer to the crossover transition of $|F=2\rangle \rightarrow |F'=1\rangle \& |F'=2\rangle$, which increases the absorption effect for σ^- polarization. The situation is reversed when the magnetic field increases in the negative direction. For the σ^- polarized beam, blue detuning leads to weakened absorption, whereas for the σ^+ polarized beam, red detuning causes the combined effect of the two couplings to enhance the absorption.

Figure 3(d) provides a more straightforward illustration of this phenomenon. We plot the normalized intensity dependence with the azimuthal angle to analyze the results more quantitatively. For $m=1$, the black triangle points in Fig. 3(d) present the transmitted intensity beam profile when $B=-5.2$ G and the purple curve gives a reversed behavior of the shape with $B=5.2$ G. It is obvious that the absorption effect can not be explained by resonant case.

Principally, the photons will be absorbed completely when the laser frequency is resonant with the atomic transition. However, due to the quantum coherence effect, the atoms can be transparent for photons with some particular polarization. This phenomenon is quite similar to the EIT effect.

As mentioned before, the phenomenon that atoms are transparent to the specific polarization state of PHVVB can be attributed to quantum coherence in atomic systems. The polarization states of neighboring regions of the PHVVB are orthogonal to each other, which results in transparency as the atoms move between these regions.

To study the spatial quantum coherence introduced by atomic motion more specifically, we measure the full width at half maximum (FWHM) of the spectrum for PHVVB with different TCs and different beam sizes. Experimentally, we apply a scanning magnetic field to the atoms by using a signal generator that produces a periodic triangular wave with an amplitude of 12 V and the aroused Zeeman level split range is from −1.2 MHz to 1.2 MHz, which can cover the transmitted spectrum width.

By selecting double-glued lenses with focal lengths of 250 mm, 400 mm, and 500 mm after the axicon, we can generate PHVVB beams with different diameters corresponding to 1.3 mm, 2.5 mm, and 3.2 mm. Figures 4(a)–4(c) show the results of the spectrum width for different beam sizes with $m=1$, $m=2$, and $m=3$, respectively. The insert figure in the upper right corner shows the transmission intensity with the Zeeman detuning. We can find that the transmission peak decreases as the beam size expands, which is consistent with the results of previous investigations.[23] The reason is that the expansion of the beam size leads to a prolonged transfer time for the atoms to establish coherence in the regions adjacent to each other with orthogonal polarization. Then, we calculate the FWHM of the spectrum by normalizing the intensity profile for different beam sizes with 1.3 mm, 2.5 mm, and 3.2 mm. The transmitted spectrums for different beam sizes are present in purple, green, and orange curves. For $m=1$, the FWHM of the purple curve (555 kHz) is smaller than that of the green (587 kHz) and orange (667 kHz) curves, which means the more considerable spatial distance can broaden the spectrum width slightly. It is reasonable because when increasing the beam diameter, the spatial quantum coherence could be effectively reconstructed by atoms with larger velocity, which will consequently induce the broadened absorption peak.

For comparison, we plot the normalized transmission spectra of beams with different TCs but fixed beam sizes, and

the results are shown in Figs. 4(d)–4(f). When keeping the beam size at 1.3 mm, the spectrum width maintains around 550 kHz regardless of TC, and the linewidth increases to about 589 kHz with a beam size of 2.5 mm and 663 kHz with a beam size of 3.2 mm. It is evident that the transmission spectral linewidth of PHVVB does not depend on the TCs. Physically, for the PHVVB with high-order TCs, the photons will imprint the higher orbital momentum to atoms, which probably increases the linewidth of the spectrum for the PHVVB. However, the measured FWHM of the spectrum for $m = 1$, $m = 2$, and $m = 3$ are nearly the same. The reason is that the momentum transferred to the atoms is not enough to affect the atom's motion, which makes the transmission peak maintain the same width.

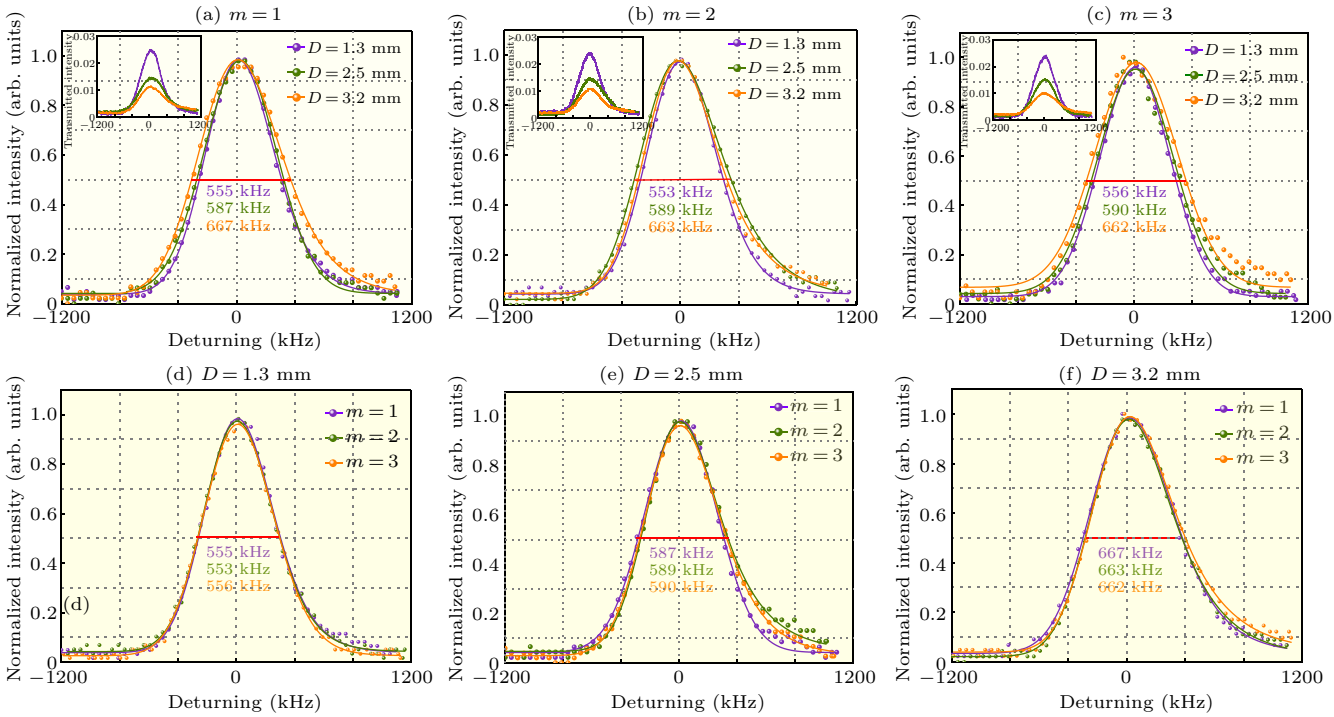


Fig. 4. The transmission spectrum of PHVVB with Zeeman detuning. Panels (a)–(c) illustrate the relationship between the transmission linewidth and the beam size with a fixed TC. Panels (d) and (e) are the results of the spectrum width for different beam sizes with $m = 1$, $m = 2$, and $m = 3$, respectively.

Moreover, the beam diameters of PHVVB with different TCs are nearly identical, thereby avoiding temporal misalignment of atomic drift during quantum coherent transmission. It is worth mentioning that the linewidth broaden effect should be considered in an even higher TC case because the momentum transferred from the photons will be comparable with the atomic motion in the radial direction. Then, the momentum collision effect cannot be neglected.

The results suggest that the spatial quantum coherence of the atomic medium is highly preserved during the PHVVB propagation, and the transmission spectrum of PHVVB can be effectively maintained regardless of variations with lower TCs. These results provide valuable insights into the quantum coherence of the PHVVB and its interaction with the atomic systems, which have potential applications for demonstrating the high-dimension coding with PHVVB in atomic ensembles.

4. Conclusion and perspectives

We investigate the spatial quantum coherent modulation of the PHVVB based on the atomic medium. We observe the absorption effect of the PHVVB with different TCs under variant magnetic fields. We find that the transmission spectrum of PHVVB can be effectively maintained regardless of variations with lower TC, but the width of the transmission peak increases as the beam size expands in hot atomic vapor because the spatial quantum coherence could be effectively constructed by atoms with larger velocities. The interaction between the PHVVB and the Rb atoms under the influence of magnetic fields presents a deeper understanding of the quantum behavior of hybrid structure beams in an atomic ensemble, which will offer promising prospects for future advancements in quantum optics and quantum sensing technologies.

Acknowledgment

Project supported by the Youth Innovation Promotion Association CAS and State Key Laboratory of Transient Optics and Photonics Open Topics (Grant No. SKLST202222).

References

[1] Naidoo D, Roux F S, Dudley A, Litvin I, Piccirillo B, Marrucci L and Forbes A 2016 *Nat. Photonics* **10** 327
[2] Hu Z, Liu H, Xia J, He A, Li H, Du Z, Chen T, Li Z and Lu Y 2020 *Appl. Opt.* **59** 9956

[3] Chen Y, Fang Z X, Ren Y X, Gong L and Lu R D 2015 *Appl. Opt.* **54** 8030

[4] Bao Y J, Ni J C and Qiu C W 2020 *Adv. Mater.* **32** 1905659

[5] Fu S Y, Wang T L and Gao C Q 2016 *Appl. Opt.* **55** 6501

[6] Liu Y C, Ke Y G, Zhou J X, Liu Y Y, Luo H L, Wen S C and Fan D Y 2017 *Sci. Rep.* **7** 44096

[7] Ostrovsky A S, Rickenstorff-Parrao C and Arrizon V 2013 *Opt. Lett.* **38** 534

[8] Xin Z Q, Zhang C L and Yuan X C 2017 *IEEE Photon. J.* **9** 7903107

[9] Liu S, Qi S X, Zhang Y, Li P, Wu D J, Han L and Zhao J L 2018 *Photonics Res.* **6** 228

[10] Sun R S, Liu T, Ren Y, Liu Z L and Li R J 2022 *Acta Opt. Sin.* **42** 2226001

[11] Ke Y G, Chen S Z, Shu W X and Luo H L 2019 *Opt. Commun.* **446** 191

[12] Liu J M, Chen X Y, He Y L, Lu L M, Ye H P, Chai G Y, Chen S Q and Fan D Y 2020 *Results Phys.* **19** 103455

[13] Li Y K, Wang J W, Yang X, Chen Y, Chen X Y, Cao M T, Wei D, Gao H and Li F L 2019 *Chin. Phys. B* **28** 014205

[14] Yang X, Fang A, Wang J, Li Y, Chen X, Zhang X, Cao M, Wei D, Muller-Dethlefs K, Gao H and Li F 2019 *Opt. Express* **27** 3900

[15] Chen Y, Wang J, Wang C, Zhang S, Cao M, Franke-Arnold S, Gao H and Li F 2021 *Opt. Express* **29** 31582

[16] Chang H, Yang X, Wang J, Ma Y, Yang X, Cao M, Zhang X, Gao H, Dong R and Zhang S 2023 *Chin. Phys. B* **32** 034207

[17] Wang J, Yang X, Li Y, Chen Y, Cao M, Wei D, Gao H and Li F 2018 *Photonics Res.* **6** 451

[18] Wang J W, Yang X, Dou Z H, Qiu S W, Liu J, Chen Y, Cao M T, Chen H X, Wei D, Muller-Dethlefs K, Gao H and Li F L 2019 *Appl. Phys. Lett.* **115** 221101

[19] Francica G, Binder F C, Guarnieri G, Mitchison M T, Goold J and Plastina F 2020 *Phys. Rev. Lett.* **125** 180603

[20] Xi Z, Li Y and Fan H 2015 *Sci. Rep.* **5** 10922

[21] Cho S U, Moon H S, Chough Y T, Bae M H and Kim N 2014 *Phys. Rev. A* **89** 053814

[22] Xiao Y H, Klein M, Hohensee M, Jiang L, Phillips F, Lukin M D and Walsworth R L 2008 *Phys. Rev. Lett.* **101** 043601

[23] Yang X, Chen Y, Wang J, Dou Z, Cao M, Wei D, Batelaan H, Gao H and Li F 2019 *Opt. Lett.* **44** 2911

[24] Qiu S W, Wang J W, Castellucci F, Cao M T, Zhang S G, Clark T W, Franke-Arnold S, Gao H and Li F L 2021 *Photonics Res.* **9** 2325

[25] Ahmed H, Ansari M A, Li Y, Zentgraf T, Mehmood M Q and Chen X 2023 *Nat. Commun.* **14** 3915

[26] Liu Y, Ke Y, Zhou J, Liu Y, Luo H, Wen S and Fan D 2017 *Sci. Rep.* **7** 44096

[27] Schaefer B, Collett E, Smyth R, Barrett D and Fraher B 2007 *Am. J. Phys.* **75** 163

[28] Milione G, Sztul H, Nolan D and Alfano R 2011 *Phys. Rev. Lett.* **107** 053601

[29] Siddons P, Adams C S, Ge C and Hughes I G 2008 *J. Phys. B: At. Mol. Opt. Phys.* **41** 155004